The Astrophysical Journal, 795:145 (12pp), 2014 November 10 doi:10.1088/0004-637X/795/2/145

KECK-I MOSFIRE SPECTROSCOPY OF COMPACT STAR-FORMING GALAXIES AT $z \gtrsim 2$: HIGH VELOCITY DISPERSIONS IN PROGENITORS OF COMPACT QUIESCENT GALAXIES

Guillermo Barro[1], Jonathan R. Trump[2,18], David C. Koo[1], Avishai Dekel[3], Susan A. Kassin[4], Dale D. Kocevski[5], Sandra M. Faber[1], Arjen van der Wel[6], Yicheng Guo[1], Pablo G. Pérez-González[7,8], Elisa Toloba[1], Jerome J. Fang[1], Camilla Pacifici[9], Raymond Simons[10], Randy D. Campbell[11], Daniel Ceverino[12], Steven L. Finkelstein[13], Bob Goodrich[11], Marc Kassis[11], Anton M. Koekemoer[4], Nicholas P. Konidaris[14], Rachael C. Livermore[13], James E. Lyke[11], Bahram Mobasher[15], Hooshang Nayyeri[15], Michael Peth[10], Joel R. Primack[16], Luca Rizzi[11], Rachel S. Somerville[17], Gregory D. Wirth[11], and Adi Zolotov[3]

[1] University of California, Santa Cruz, 1156 High Street, Santa Cruz, CA 95064, USA
[2] Pennsylvania State University, University Park, State College, PA 16802, USA
[3] Racah Institute of Physics, The Hebrew University, Jerusalem 91904, Israel
[4] Space Telescope Science Institute, 3700 San Martin Drive, Baltimore, MD 21218, USA
[5] University of Kentucky, Lexington, KY 40506, USA
[6] Max-Planck-Institut für Astronomie, Königstuhl 17, D-69117 Heidelberg, Germany
[7] Universidad Complutense de Madrid, Avda. de Sneca, 2 Ciudad Universitaria, E-28040 Madrid, Spain
[8] Steward Observatory, University of Arizona, 933 North Cherry Avenue, Tucson, AZ 85721-0065, USA
[9] Yonsei University Observatory, Yonsei University 50, Yonsei-ro, Seodaemun-gu, Seoul 120-749, Korea
[10] Johns Hopkins University, 3400 N. Charles Street, Baltimore, MD 21218-2683, USA
[11] W. M. Keck Observatory, California Association for Research in Astronomy, 65-1120 Mamalahoa Highway, Kamuela, HI 96743, USA
[12] Universidad Autonoma de Madrid, Ciudad Universitaria de Cantoblanco, E-28049 Madrid, Spain
[13] The University of Texas at Austin, Austin, TX 78712, USA
[14] California Institute of Technology, 1200 E. California Blvd, Pasadena, CA 91125, USA
[15] University of California, Riverside, 900 University Avenue, CA 92521, USA
[16] Santa Cruz Institute for Particle Physics, UC Santa Cruz, 1156 High Street, Santa Cruz, CA 95064, USA
[17] Rutgers University, Rutgers, The State University of New Jersey, 57 US Highway, 1 New Brunswick, NJ 08901-8554, USA
Received 2014 May 28; accepted 2014 September 15; published 2014 October 23

ABSTRACT

We present Keck-I MOSFIRE near-infrared spectroscopy for a sample of 13 compact star-forming galaxies (SFGs) at redshift $2 \leqslant z \leqslant 2.5$ with star formation rates of SFR $\sim 100\,M_{\odot}\,\mathrm{yr}^{-1}$ and masses of $\log(M/M_{\odot}) \sim 10.8$. Their high integrated gas velocity dispersions of $\sigma_{\rm int} = 230^{+40}_{-30}\,\mathrm{km\,s}^{-1}$, as measured from emission lines of Hα and [O III], and the resultant $M_{\star}$–$\sigma_{\rm int}$ relation and $M_{\star}$–$M_{\rm dyn}$ all match well to those of compact quiescent galaxies at $z \sim 2$, as measured from stellar absorption lines. Since $\log(M_{\star}/M_{\rm dyn}) = -0.06 \pm 0.2$ dex, these compact SFGs appear to be dynamically relaxed and evolved, i.e., depleted in gas and dark matter ($<13^{+17}_{-13}\%$), and present larger $\sigma_{\rm int}$ than their non-compact SFG counterparts at the same epoch. Without infusion of external gas, depletion timescales are short, less than ∼300 Myr. This discovery adds another link to our new dynamical chain of evidence that compact SFGs at $z \gtrsim 2$ are already losing gas to become the immediate progenitors of compact quiescent galaxies by $z \sim 2$.

Key words: galaxies: high-redshift – galaxies: photometry – galaxies: starburst

Online-only material: color figures

1. INTRODUCTION

The formation scenario for the first massive quiescent galaxies is still unclear. While observations report a rapid increase in the number density of massive galaxies with suppressed star formation rates (SFRs) since $z \sim 3$ (Brammer et al. 2011; Whitaker et al. 2011; Muzzin et al. 2013), other surprising results, such as their remarkably small (∼1 kpc scale) sizes (Trujillo et al. 2007; Buitrago et al. 2008; Cimatti et al. 2008; van Dokkum et al. 2008; Cassata et al. 2011; Szomoru et al. 2012) and their large velocity dispersions (van Dokkum et al. 2008; Cappellari et al. 2009; Newman et al. 2010; Toft et al. 2012; van de Sande et al. 2013; Bezanson et al. 2013; Belli et al. 2014a) in comparison with local galaxies of the same stellar mass pose a puzzle as to which galaxies are their immediate star-forming progenitors. Given that galaxy structure and kinematics appear to be more robust and stable properties than luminosity or SFR (e.g., Franx et al. 2008; Wake et al. 2012; Bell et al. 2012; Cheung et al. 2012), it is unlikely that the typical massive star-forming galaxies (SFGs) at $z \sim 2$, which consist mostly of extended disks (Wuyts et al. 2011b; Buitrago et al. 2013) with irregular, sometimes clumpy, morphologies and have high rotational velocities (Elmegreen et al. 2004; Elmegreen & Elmegreen 2005; Genzel et al. 2008, 2012; Law et al. 2009, 2012; Förster Schreiber et al. 2009, 2011; Wuyts et al. 2012; Swinbank et al. 2012a, 2012b; Guo et al. 2012) are the progenitors of compact quiescent galaxies. Instead, it is more plausible that their precursors are similarly compact SFGs. These compact SFGs probably formed in strongly dissipative gas-rich processes, such as mergers (Hopkins et al. 2006; Naab et al. 2007; Wuyts et al. 2010) or accretion-driven disk instabilities (Dekel et al. 2009; Dekel & Burkert 2014; Ceverino et al. 2010) which contracts the galaxy, producing a compact, dispersion-dominated, remnant (Dekel & Burkert 2014). Alternatively, some of these galaxies could have been compact since their formation epoch, growing mostly in stellar mass with only moderate size evolution, i.e., building up the stellar core of low-mass ($\log(M/M_{\odot}) \lesssim 10$) seed galaxies (Williams et al. 2014a; Feldmann & Mayer 2014).

[18] Hubble Fellow.

A crucial step forward in determining what are the most likely progenitors of compact quiescent galaxies is the recent discovery of a population of massive ($\log(M/M_\odot) > 10.3$), *compact* dusty SFGs at $z \gtrsim 2$ (Wuyts et al. 2011b; Barro et al. 2013; Patel et al. 2013; Stefanon et al. 2013). In Barro et al. (2013, 2014) we showed that compact SFGs have dust-obscured spectral energy distributions (SEDs) characterized by bright IR fluxes (∼70% and 30% are detected by *Spitzer* and *Herschel* in the far-IR) that, nonetheless, translate into seemingly *normal* SFR ∼ 100–200 $M_\odot\,\mathrm{yr}^{-1}$, different from those of extreme submillimeter (sub-mm) galaxies (Bothwell et al. 2013; Toft et al. 2014). Structurally, they present centrally concentrated, spheroidal morphologies and high Sérsic indices consistent with those of compact quiescent galaxies, and they follow a similar mass–size relation. In addition, we found that the observed number density of compact SFGs can reproduce the build up of the compact quiescent population since $z \sim 3$, if they quench star formation in a few 10^8 yr. This led us to propose an evolutionary picture in which compact SFGs are formed from larger SFGs as a result of gas-rich processes (mergers or disk instabilities) that induce a compact starburst which quench on dynamical timescales fading into a compact quiescent galaxy. So far the similarities between compact SFGs and quiescent galaxies are already very encouraging. However, they are based on photometric and structural properties and thus have yet to be verified from kinematic data to confirm the connection.

This paper presents near-infrared (NIR) spectroscopic follow-up of a sample of massive compact SFGs at $2 \leqslant z \leqslant 3$ presented in Barro et al. (2013, 2014) to measure their kinematic properties and compare them against those of compact quiescent galaxies to test whether they support the picture of a rapid fading into the red sequence. We also estimate stellar and dynamical masses for compact SFGs to infer their gas fractions and gas depletion timescales, and we analyze their stacked spectra for signs of outflowing gas. While several other surveys have already presented emission-line measurements and kinematic properties for SFGs at $z \gtrsim 1.5$ (Erb et al. 2006; Law et al. 2007, 2009; Förster Schreiber et al. 2009; Epinat et al. 2012; Newman et al. 2013; Masters et al. 2014; Buitrago et al. 2014; Williams et al. 2014b), this is the first observational effort to target specifically massive, yet small, compact SFGs, which may be notoriously missing in those surveys (although see the recent Genzel et al. 2014; Nelson et al. 2014).

Throughout the paper, we adopt a flat cosmology with $\Omega_M = 0.3$, $\Omega_\Lambda = 0.7$ and $H_0 = 70\,\mathrm{km\,s^{-1}\,Mpc^{-1}}$ and we quote magnitudes in the AB system.

2. DATA AND SAMPLE SELECTION

Our targets are compact SFGs at $z \gtrsim 2$ to be measured for kinematic properties using their emission lines. These galaxies, first identified in Wuyts et al. (2011b) and Barro et al. (2013), have been proposed to be the immediate precursors of compact quiescent galaxies at $z \sim 2$ as they share structural properties while spanning a range in SFRs, from main sequence to almost quenched (Barro et al. 2014).

2.1. Photometric Data, Stellar Properties, and SFRs

We select galaxies from the CANDELS (Grogin et al. 2011; Koekemoer et al. 2011) WFC3/F160W (H-band) multi-wavelength catalogs in GOODS-S, GOODS-N, and COSMOS (Guo et al. 2013; G. Barro et al. in preparation; H. Nayyeri et al. in preparation). The galaxy SEDs include extensive multi-band data ranging from the UV to the NIR. We also include complementary mid-IR photometry in *Spitzer*/MIPS 24 and 70 μm (30 μJy and 1 mJy, 5σ) from Pérez-González et al. (2008), and far-IR from the GOODS-*Herschel* (Elbaz et al. 2011) and PACS evolutionary probe (Magnelli et al. 2013) surveys. For each galaxy, we fit photometric redshifts using EAzY (Brammer et al. 2008) and calculate stellar masses using FAST (Kriek et al. 2009), assuming Bruzual & Charlot (2003) stellar population synthesis models, a Chabrier (2003) initial mass function (IMF), and the Calzetti et al. (2000) dust extinction law with attenuations ranging between $0 < A_V < 4$. We assume an exponentially declining star formation history with timescale τ and age t. Following Wuyts et al. (2011a) we impose a soft constraint on the minimum e-folding time ($\log \tau > 8.5$) to obtain better agreement between different SFR indicators (see below). Age is allowed to vary over the range $10\,\mathrm{Myr} < t < t_H$, where t_H is the age of the universe at the given redshift.

We follow the method of the SFR-*ladder* as described in Wuyts et al. (2011a) to obtain consistent SFRs over a broad dynamic range. In brief, for galaxies detected at mid-to-far-IR wavelengths (i.e., *Spitzer*/MIPS and *Herschel*/PACS) we compute the total SFR by adding the unobscured and obscured star formation, traced by the UV and IR emission, respectively, following Kennicutt (1998; see also Bell et al. 2005):

$$\mathrm{SFR_{UV+IR}} = 1.09 \times 10^{-10}(L_\mathrm{IR} + 3.3\,L_{2800})(M_\odot\,\mathrm{yr}^{-1}), \quad (1)$$

where L_IR is the total IR luminosity ($L_\mathrm{IR} \equiv L(8\text{–}1000\,\mu\mathrm{m})$) derived from the fit to *Spitzer* and *Herschel* data, and L_{2800} is estimated from the best-fitting SED template. The normalization factor corresponds to a Chabrier (2003) IMF. For galaxies undetected in the IR ($\mathrm{SFR_{IR+UV}} \lesssim 30\,M_\odot\,\mathrm{yr}^{-1}$) we correct $\mathrm{SFR_{UV}}$ for extinction using the attenuation derived from the best-fit SED model. This method has been shown to provide consistent SFR estimates down to very low specific star formation rate (sSFR) levels ($\log(\mathrm{sSFR/Gyr^{-1}}) > -1$; Wuyts et al. 2011a; Fumagalli et al. 2013; Utomo et al. 2014). In practice, we used $\mathrm{SFR_{IR+UV}}$ for all compact SFGs described in the next section, as they are all detected in MIPS 24 μm and ∼30% in PACS.

X-ray source identifications and total luminosities ($L_\mathrm{X} \equiv L_{0.5-8\mathrm{kev}}$) were computed for the sources identified in the *Chandra* 4 *Ms* and 2 *Ms* catalogs in GOODS-S (Xue et al. 2011) and GOODS-N (Alexander et al. 2003), respectively.

The shape of the two-dimensional (2D) surface brightness profiles measured from the *Hubble Space Telescope*/WFC3 F160W image were modeled using GALFIT (Peng et al. 2002). The effective (half-light) radius and the Sérsic index, n are determined using a single component fit. Position dependent point-spread functions (PSFs) are created and processed with TinyTim (Krist 1995) to replicate the conditions of the observed data when fitting light profiles. The method and the catalog of morphological properties are fully described in van der Wel et al. (2012). The stellar and star-formation properties have been previously used in several other papers (Wuyts et al. 2011b; Barro et al. 2013, 2014; Trump et al. 2013).

2.2. Selection of Compact and Extended SFGs

We select compact SFGs following the method described in Barro et al. (2013, 2014). Briefly, we require galaxies to be star forming by having $\log(\mathrm{sSFR/Gyr^{-1}}) > -0.65$, corresponding to a mass doubling time of a few times the age of the universe at $z \sim 2$. We define compactness using a threshold in *pseudo* stellar

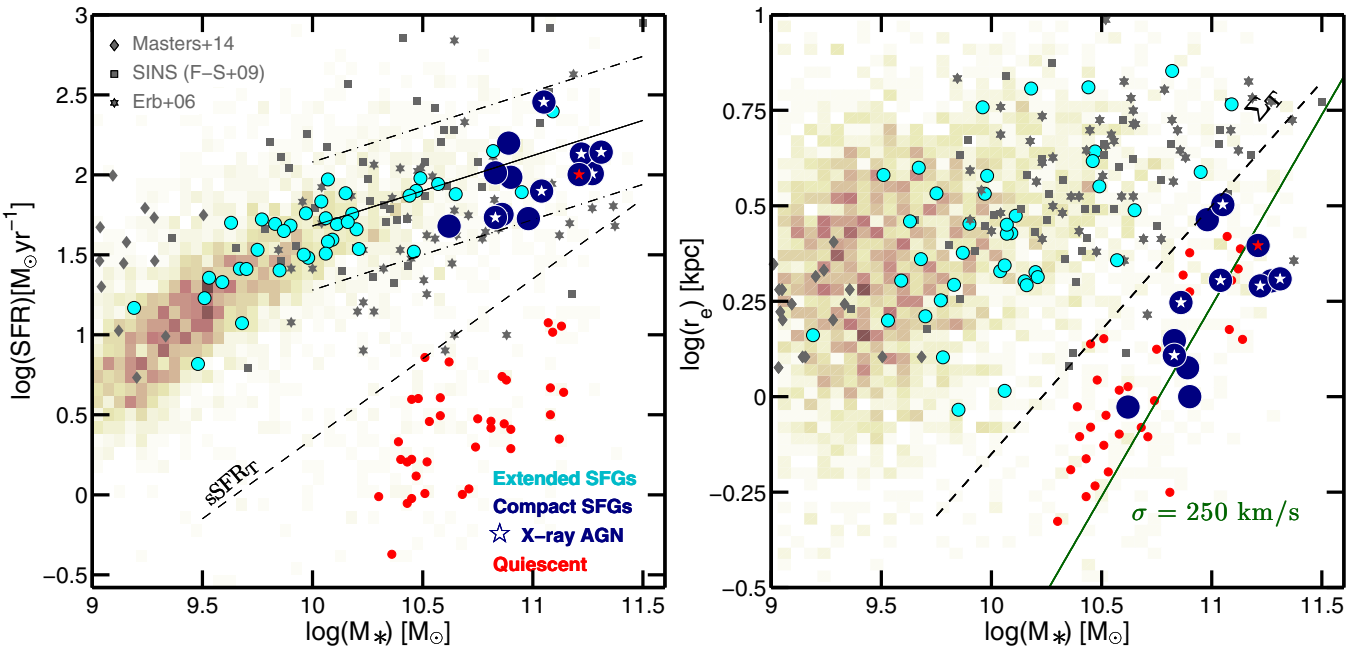

Figure 1. Left panel: SFR–mass diagram for all galaxies in the parent galaxy catalog in GOODS-S and GOODS-N at $2 < z < 3$. The checkered gray scale illustrates the location of the star-forming main sequence. The solid and dashed–dotted lines depict the best-fit and 1σ scatter to the massive end ($\log(M/M_\odot) > 10$) of the main sequence. The 13 compact and 67 extended SFGs observed with NIR spectroscopy are shown in blue and cyan colors, respectively. X-ray-detected galaxies are indicated with a white star symbol. The red star depicts the galaxy in common with Belli et al. (2014b, see Section 4.3). The dashed line illustrates the selection threshold in sSFR ($\log(\mathrm{sSFR/Gyr^{-1}}) < -0.65$). The red markers show the quiescent population. Right panel: mass–size distribution for the same galaxies in the left panel. The dashed line illustrates the compactness threshold ($\Sigma_{1.5} = 10.4\,M_\odot\,\mathrm{kpc}^{-1.5}$). The green line shows the expected location of galaxies with constant velocity dispersion $\sigma = 250\,\mathrm{km\,s^{-1}}$, as inferred from Equation (3), assuming $M_{\rm dyn} = M_\star$. These panels illustrate our selection criteria for compact SFGs aimed at identifying normal main-sequence SFGs following a more compact mass–size relation, similar to that of the quiescent population.

(A color version of this figure is available in the online journal.)

mass surface density of $\Sigma_{1.5} = \log(M/r_e^{1.5}) > 10.4\,M_\odot\,\mathrm{kpc}^{-1.5}$. Figure 1 illustrates this selection showing the location of the 13 compact SFGs (blue circles) observed with MOSFIRE overlaid in the SFR–mass and mass–size diagrams for galaxies more massive than $\log(M/M_\odot) > 9$ at $2 < z < 3$ in the CANDELS GOODS-N and GOODS-S catalogs. The compactness criterion selects SFGs that follow a mass–size relation similar to that of the quiescent population. As shown in Newman et al. (2012; see also Cassata et al. 2013; van der Wel et al. 2014), quiescent galaxies follow a tight mass–size relation with a slope, $\alpha \sim 1.5$, that remains constant with redshift, and a mass-normalized radius that evolves with $(1+z)^{0.025}$.

In order to discuss the properties of compact SFGs in the general context of SFGs at $z \sim 2$, Figure 1 shows a sample of 67 extended SFGs ($\Sigma_{1.5} < 10.4$; cyan circles), also observed in our MOSFIRE survey, and other SFGs at $z \gtrsim 1.4$–2.5 drawn from Erb et al. (2006), Förster Schreiber et al. (2009), Maseda et al. (2013), and Masters et al. (2014). It is clear from the figure that, while compact SFGs lie in the same locus of the SFR–mass diagram as other SFGs, they occupy a distinct region of the mass–size diagram under-represented in previous surveys of SFGs. For simplicity, in the remainder of the paper we use the term extended SFGs to describe both our extended SFGs and those from the reference samples, which also have $\Sigma_{1.5} < 10.4$.

3. MOSFIRE NIR SPECTROSCOPY

We conducted NIR spectroscopic observations in GOODS-S using the new multi-object spectrograph MOSFIRE (McLean et al. 2010, 2012) on the Keck-I Telescope. The data were taken in four runs on 2012 September 14–15, October 10, 2013 December 25–28, and 2014 January 1–2. We observed a total of eight masks in the H-band ($1.46 < \lambda < 1.81\,\mu$m) and three masks in three K-band ($1.93 < \lambda < 2.41\,\mu$m), with exposure times ranging between 50–120 minutes and 40–100 minutes, respectively. Overall, the weather conditions were excellent with seeing $\sim$0.″4–0.″6 and good transparency in all the masks except for two in the K-band, for which the seeing was poor ($\gtrsim$1″) and there were partial clouds. We used the same observational configuration for all masks: two-point dithers separated by 1.″5 and slit widths of 0.″7. The instrumental resolution of MOSFIRE with 0.″7 slit widths is approximately $R = 3200$ ($\sim$5 Å per resolution element). Two-dimensional spectra were reduced, sky subtracted, wavelength calibrated, and one dimensionally extracted using the public MOSFIRE data reduction pipeline. Redshifts were found using the Specpro software (Masters & Capak 2011). We also include in this paper SFGs observed as a part of the TKRS2 survey, which observed the GOODS-N field in the J-, H,- and K-bands in three runs on 2012 December 27 and January 14, and 2013 May 3 (see G. D. Wirth, in preparation, for details on the overall target selection and observing strategy), and one K-band mask in COSMOS observed for 60 minutes in 2014 March 14 (PI: Finkelstein). The data were reduced following the same procedure as in our main program.

Overall each MOSFIRE mask includes 25 galaxies out of which only a small fraction is discussed in this paper. Our primary targets are 13 compact SFGs and 67 extended SFGs at $z = 1.8$–2.4. The latter were selected to study the excitation properties of active galactic nuclei (AGNs) and the kinematic properties of clumpy SFGs (see Trump et al. 2013 for more details on these galaxies). Here we used those galaxies mostly

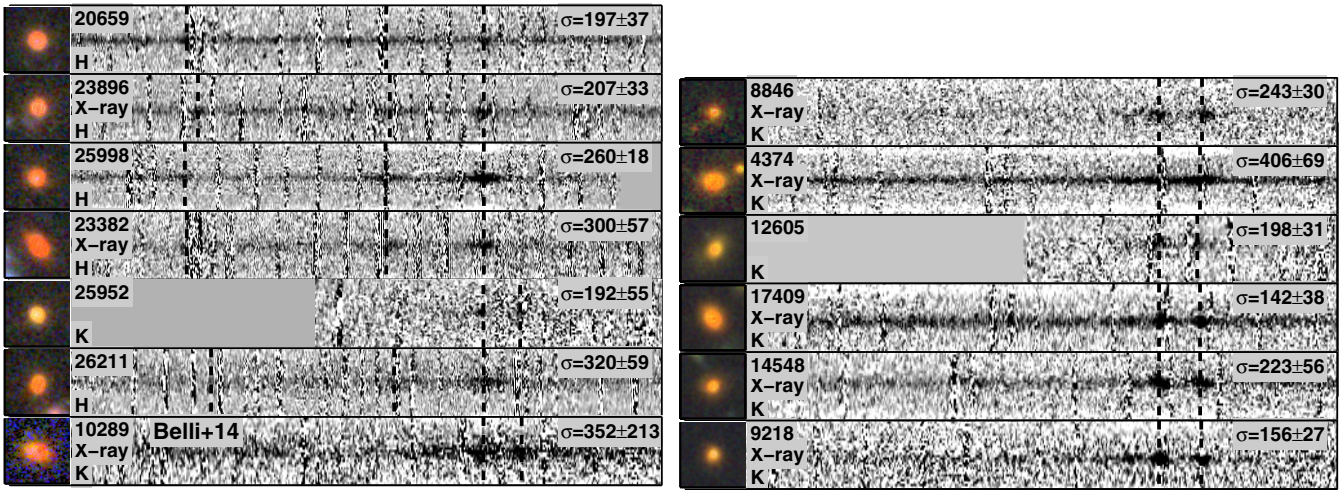

Figure 2. Two-dimensional MOSFIRE *H*- and *K*- spectra of the 13 compact SFGs jointly with their 3″ × 3″ ACS/WFC3 *zJH* color composite postage stamps. Compact SFGs have strikingly red rest-frame UV–optical colors due to their high dust obscuration. The black dashed lines indicate the most prominent emission lines, either Hα and/or O III and Hβ with increasing wavelength to the right (see also Figure 3 for more details). Compact SFGs are barely resolved in the spatial direction. Only 17409 and 14548 show a hint of resolved kinematics. The measured $\sigma_{\rm int}$ and the X-ray detected galaxies are indicated in the text.

(A color version of this figure is available in the online journal.)

for comparison purposes to illustrate the differences relative to compact SFGs.

4. DYNAMICAL PROPERTIES OF COMPACT SFGs

4.1. Kinematic Measurements

Here we assume that the emission-line velocity dispersions are primarily due to the motion of the gas in the gravitational potential of the galaxy. Nevertheless, in the following sections, we also discuss the possible caveats in this assumption due to the presence of an AGN or to the effects of turbulence and outflows. The integrated velocity dispersion, $\sigma_{\rm int}$, can be determined for all galaxies because it requires only a measurement of the width of the emission line. It is therefore the most straightforward and useful kinematic quantity. Note that, even in the best seeing conditions (∼0.″4), compact SFGs are barely resolved in the spatial direction (Figure 2; see also Section 4.6). Thus $\sigma_{\rm int}$ could represent either the intrinsic σ of the galaxy, the collapsed $v_{\rm rot}$ of a small rotating disk, or a combination of the two.

We determine the one-dimensional (1D) velocity dispersion by fitting a Gaussian profile to each emission line, measuring its FWHM, and subtracting the instrumental broadening in quadrature from the FWHM (following Weiner et al. 2006 and Kassin et al. 2007). We use the highest signal-to-noise ratio (S/N) line available in the *H*- and *K*-band spectra, which are either O III 5007 Å or Hα, respectively. The second O III 4959 Å and H$_\beta$ lines are rarely detected with high S/N. However, for four galaxies the N II line is clearly detected in the *K*-band, and we verified that the inferred $\sigma_{\rm int}$ is consistent with the Hα value within the uncertainty of the measurement. The instrumental broadening is measured from the widths of skylines and is 2.7 Å (∼49 km s^{-1}) and 3.4 Å (∼47 km s^{-1}) in the *H*- and *K*-bands (in the observed frame), respectively. The velocity dispersion is then the corrected FWHM divided by 2.355. The whole sample of compact SFGs consists of 13 galaxies with velocity dispersions ranging from $\sigma_{\rm int}$ = 140–400 km s^{-1} and an average value of $\sigma_{\rm int} = 230^{+40}_{-30}$ km s^{-1}. For the 67 extended galaxies, the velocity dispersions are typically lower, ranging from $\sigma_{\rm int}$ = 66–150 km s^{-1}. Many of the extended galaxies are spatially resolved at the average seeing of the observations, and thus their rotational and dispersion components can be estimated from the 2D spectra. These results will be presented in R. Simons et al. (2014, in preparation). Here we adopt the $\sigma_{\rm int}$ values to provide a homogeneous kinematic measurement for all galaxies.

4.2. Kinematics of AGN Hosts

More than half of the compact SFGs are detected in the X-rays (7/13), and have large X-ray luminosities $L_{\rm X} > 10^{43}$ erg s^{-1} which suggest the presence of an AGN. This could cause a potential bias on the measured line widths, as AGN-ionized gas in the "narrow line region" (NLR) is typically dominated by emission nearer the center of a galaxy. Even though this gas is usually dominated by the gravitational potential of the galaxy rather than the AGN itself, it has broader velocities than gas at the larger effective radius.

The seven X-ray detected galaxies, however, do not have systematically broader velocity dispersions than the X-ray undetected galaxies. Instead, their median $\sigma_{\rm int}$ = 200 km s^{-1}, fully consistent with that of the non-X-ray detected compact SFGs. This is perhaps unsurprising, as their X-ray luminosities are roughly at the detection threshold of the X-ray data at $z \sim$ 2–3, rather than at large, QSO-like, values ($L_{\rm X} > 10^{44}$ erg s^{-1}). We also find no evidence for either UV excess or IR excess, traced by the IRAC bands ([8.0]/[3.6] $\lesssim$ 1.3; Donley et al. 2007, 2012), as a result of the AGN emission and, for the five *Herschel*/PACS detected galaxies, the median far-IR colors, [160]/[24] = 40, are fully consistent with star formation (Kirkpatrick et al. 2013; Barro et al. 2014). The only exception is galaxy 10289 which appears to have an elevated 8 μm flux indicative of hot dust emission near the AGN (we discuss this galaxy in the next section). Overall, these tests suggest that the AGN does not have a strong effect on the SED or the line widths inferred from it.

The ratios between partially ionized forbidden lines and recombination lines also suggest that compact SFGs are not strongly AGN-dominated. While we only have both [O III]/Hβ and [N II]/Hα for one galaxy to calculate the full Baldwin, Phillips, & Terlevich diagram (Baldwin et al. 1981), we do have [N II]/Hα alone for all but two galaxies. If we combine this

Table 1
Stellar and Spectroscopic Properties of Compact SFGs

ID (1)	R.A. (2)	Decl. (3)	z_{spec} (4)	log $M_\star$ (5)	$f_{24\,\mu m}$ (6)	$f_{100\,\mu m}$ (7)	$f_{160\,\mu m}$ (8)	SFR (9)	r_{eff} (10)	σ_{int} (11)	[NII]/Hα (12)	log M_{dyn} (13)	L_X (14)
20659	53.182839	−27.734911	2.432	10.90	72	...	...	96	1.00 ± 0.01	197 ± 37	0.77 ± 0.30	10.65 ± 0.26	...
23896	53.100814	−27.715986	2.303	10.86	49	...	...	57	1.76 ± 0.05	207 ± 33	0.17 ± 0.59	10.94 ± 0.23	0.24
25998	53.137572	−27.700104	2.453	10.89	140	3359	6716	158	1.19 ± 0.03	260 ± 18	1.70 ± 0.78	10.97 ± 0.10	...
23382	53.162299	−27.712135	2.433	11.27	80	...	2175	102	2.01 ± 0.03	300 ± 57	...	11.32 ± 0.27	0.20
25952	53.121136	−27.698075	1.970	10.62	91	...	...	48	0.94 ± 0.02	192 ± 55	0.57 ± 0.49	10.60 ± 0.41	...
26211	53.065952	−27.701852	2.154	10.83	153	1738	...	103	1.40 ± 0.02	320 ± 59	...	11.22 ± 0.26	...
8846	189.026369	62.209125	2.487	11.22	115	1477	6057	135	1.95 ± 0.14	243 ± 30	0.73 ± 0.18	11.13 ± 0.19	1.68
4374	189.028576	62.172614	2.321	11.31	107	...	6858	139	2.04 ± 0.03	406 ± 69	2.17 ± 0.28	11.59 ± 0.24	0.21
12605	189.087068	62.237622	2.090	10.98	96	832	...	53	2.91 ± 0.10	198 ± 31	0.74 ± 0.18	11.12 ± 0.22	...
17409	189.182966	62.272470	2.322	11.05	55	1181	2833	316	3.19 ± 0.02	141 ± 38	0.89 ± 0.39	10.87 ± 0.38	0.51
14548	189.251901	62.252460	2.330	11.04	84	...	1937	79	2.02 ± 0.06	223 ± 56	0.92 ± 0.30	11.07 ± 0.35	0.74
9218	189.260847	62.212224	2.420	10.83	64	...	...	54	1.28 ± 0.03	156 ± 27	0.23 ± 0.39	10.56 ± 0.24	2.47
10289	150.074608	2.302008	2.095	11.21	220	...	...	110	2.09 ± 0.05	352 ± 213	<0.5	11.39 ± 045	1.67

Notes. (1) General ID in the CANDELS *H*-band selected catalog in GOODS-S (Guo et al. 2013), GOODS-N (G. Barro et al. in preparation), and COSMOS (H. Nayyeri et al. in preparation) catalogs. ((2) and (3)) R.A and declination J2000. (4) Spectroscopic redshift. (5) Stellar mass ($\log(M/M_\odot)$) determined from SED fitting using Bruzual & Charlot (2003). ((6)–(8)) Far-IR fluxes in *Spitzer*/MIPS 24 μm and *Herschel*/PACS 100 μm and PACS 160 μm. (9) Total star formation rate (SFR_{UV+IR} ($M_\odot\,yr^{-1}$)); see Section 2.1. (10) Circularized, effective (half-light) radius (kpc) measured with GALFIT; see Section 2.1. (11) Integrated velocity dispersion measure from the line width (FWHM); see Section 4.1. (12) [NII] to Hα line ratio. (13) Dynamical mass estimated from the velocity dispersion and effective radius of the galaxy; see Section 4.4. (14) Full band X-ray luminosity in units of 10^{44} erg s^{-1}.

[NII]/Hα with a conservative, but elevated, [O III]/H$\beta \sim 5$, similar to values reported in recent papers (Trump et al. 2011; Holden et al. 2014; Steidel et al. 2014), these galaxies would lie predominantly in the mixed AGN–star-forming region with $0.2 \leqslant$ [NII]/H$\alpha \leqslant 1$ values (see Table 1). Only two galaxies present [NII]/Hα ratios significantly larger than one (25998 and 4374), and both of them are clearly detected by *Herschel* indicating ongoing star formation. In fact, 4374, which presents the largest σ_{int} of the sample, is a sub-mm galaxy (see, e.g., Laird et al. 2010; Michałowski et al. 2012).

Interestingly, even if the emission lines are partially fueled by the AGN rather than star formation, these galaxies are so compact that the AGN NLR probably corresponds to the whole galaxy. For example, Bennert et al. (2002) show that the size of the NLR correlates with the O III luminosity, reaching sizes $r_{NLR} > 1$ kpc for $L_{[O\,III]} \sim 10^{42}$ erg s^{-1}, which is consistent with the expected values for these strongly SFGs with enhanced [O III]/Hβ ratios. For five compact SFGs with clear O III and continuum detections we estimate the equivalent width and the line flux using the observed flux in F160W to calibrate the continuum. The inferred O III luminosities range from $L_{[O\,III]} = 2.3$–4.5×10^{42} erg s^{-1} suggesting that their line widths are still good tracers of the potential well.

4.3. Kinematics of Compact SFGs and Quiescent Galaxies

In order to study whether the similarities between compact SFGs and quiescent galaxies extend beyond their stellar masses and structural properties, Figure 4 compares the integrated kinematics versus mass for both populations. Quite remarkably, compact SFGs occupy the same region of the diagram, following an $M_\star$ –σ_{int} relation over more than 1 dex in stellar mass similar to that of a compilation of compact quiescent galaxies at $1.5 \leqslant z \lesssim 2$ drawn from van de Sande et al. (2013) and Belli et al. (2014a, 2014b). The σ_{int} values in quiescent galaxies are measured from absorption lines and therefore use stars instead of gas as a tracer of the gravitational potential. This could potentially introduce systematic offsets if gas and stars present different motions due to shocks or turbulence, or if they are located in different regions of the galaxy. However, the striking similarity in the distribution of both populations suggest that compact SFGs are in fact kinematically relaxed (i.e., σ_{int} traces the gravitational potential) and their integrated properties match those of quiescent galaxies.

Obtaining more conclusive evidence of the matching kinematic properties of compact SFGs and quiescent requires comparing emission- and absorption-line measurements of the same galaxies. This is observationally very challenging because (1) it requires long integrations to detect absorption lines at $z \sim 2$, and (2) absorption surveys target only quiescent galaxies without emission lines. However, recent observations by Belli et al. (2014b) present absorption-line kinematics for one compact SFGs in our sample (10289; marked with a red star in all figures), and the dispersion values are consistent within the 1σ errors, $\sigma_{abs} = 312 \pm 65$ km s^{-1} versus $\sigma_{int} = 357 \pm 213$ km s^{-1}. The uncertainty in the emission-line measurement is larger due to the shorter integration time and the likely dusty nature of the galaxy. However, the Hα broadening is apparent in both the 2D and 1D spectra, and the peak of the emission line lies clearly between the strong sky lines (Figures 2 and 3). The galaxy presents an IR excess at $\lambda_{rest} = 3\,\mu$m, likely coming from the AGN, that suggests that the IR-based SFR is overestimated. Nevertheless, the SED fit also suggests an elevated dust extinction ($A_V = 2.0$) and a UV-based SFR $= 80\,M_\odot\,yr^{-1}$above the sSFR selection threshold for SFGs.

Figure 4 also reveals that extended SFGs tend to deviate from the $M_\star$–σ_{int} relation of compact galaxies having larger σ_{int} at a given stellar mass, particularly at $\log(M/M_\odot) \lesssim 10$. The black line shows the best-fit $M_\star$–σ_{int} relation for compact SFG and quiescent galaxies ($\log(\sigma_{int}) = (1.91 \pm 0.07) + (0.49 \pm 0.04)\,(\log(M/M_\odot) - 10)$; $\Delta\log(\sigma_{int}) = 0.14$ dex), which presents a steeper slope than the local Faber–Jackson relation (Faber & Jackson 1976; Gallazzi et al. 2006), as also noted in Belli et al. (2014a). Extended (disk-dominated) galaxies are often represented in the $M_\star$–v_{rot} Tully–Fisher relation (Tully & Fisher 1977). However, using a value that accounts for both rotation and velocity dispersion, such as σ_{int}, they can be shown together with other galaxies in a more fundamental

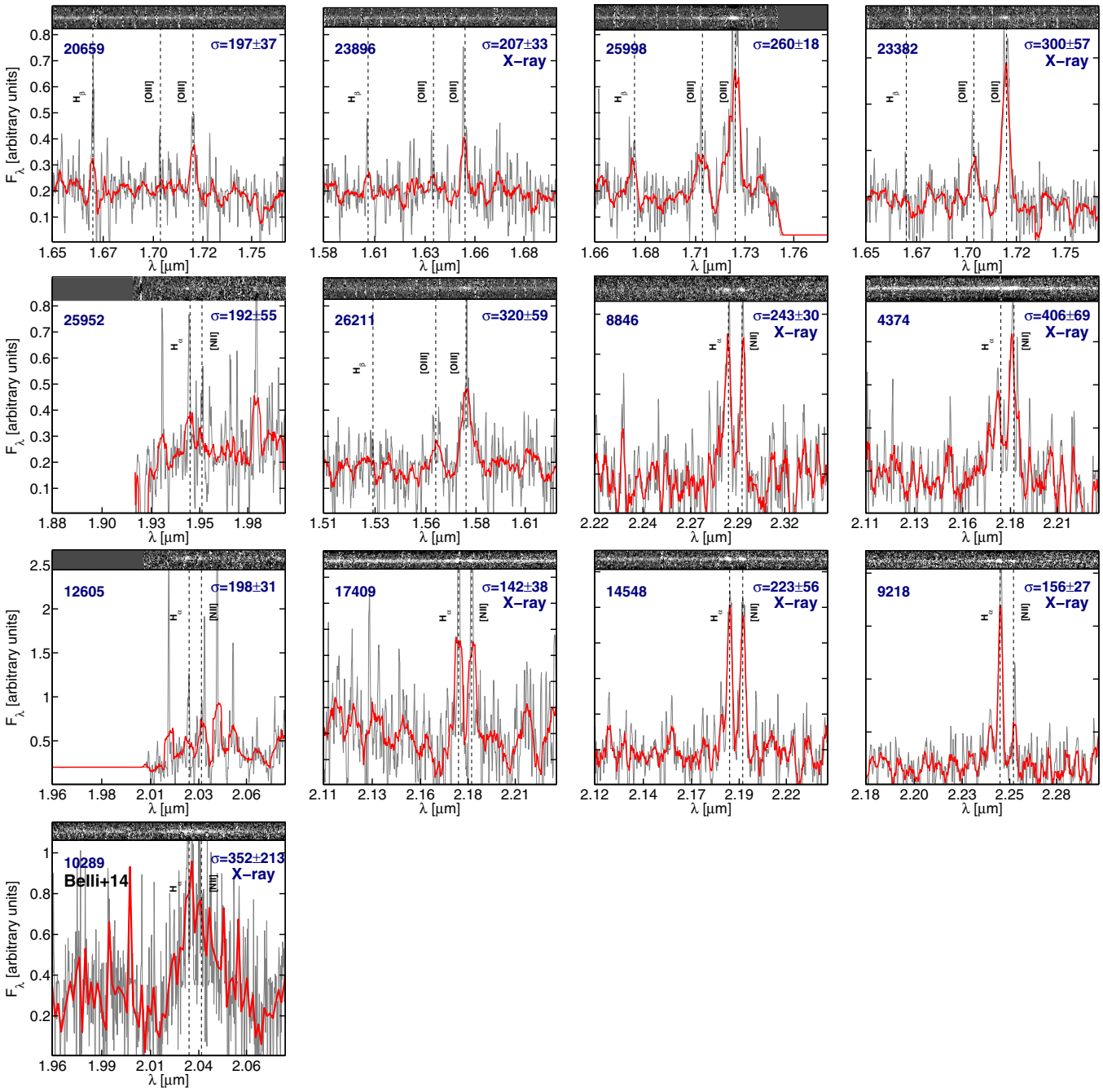

Figure 3. One-dimensional MOSFIRE *H*- and *K*-spectra of the 13 compact SFGs. Their ID, $\sigma_{\rm int}$, and detection in X-rays is indicated. The gray line shows the collapsed 1D spectra extracted from the 2D spectra shown in Figure 2. The red line shows the binned 1D spectra. The dashed lines indicate the most prominent emission lines in the observed spectral range. The last row shows the spectra of the galaxy in common with the sample of quiescent galaxies of Belli et al. (2014b).

(A color version of this figure is available in the online journal.)

relation that is a tracer of the total dynamical mass of the galaxy (e.g., Weiner et al. 2006; Kassin et al. 2007; Cappellari et al. 2013; Courteau et al. 2014). In that context, the trend in low-mass extended SFGs could indicate that $\sigma_{\rm int}$ is not only gravitational (i.e., there are turbulent motions), or perhaps that $\sigma_{\rm int}$ overestimates the intrinsic contributions from rotation and dispersion. Alternatively, extended SFGs could indeed follow a shallower $M_\star$–$\sigma_{\rm int}$ relation because they have different dynamical masses than the more massive compact galaxies, i.e., they may have a larger contribution of dark matter or gas mass to the gravitational potential, thus increasing the velocity dispersion beyond the expected value if $M_{\rm dyn} \sim M_\star$.

4.4. Dynamical Masses

In this section we make the operational assumption that compact SFGs are dispersion dominated galaxies in order to calculate dynamical masses. This is motivated by their elevated Sérsic indices ($n \sim 3.4$) and the similarities in their structural and kinematic properties with compact quiescent galaxies ($r_{\rm e} \sim 1.5$ kpc; axis ratio ~ 0.75) for which this is the usual assumption (although see van der Wel et al. 2011 and Chang et al. 2013 for evidence that some massive quiescent galaxies may be disks).

For dispersion-dominated galaxies, a simple virial argument allows one to relate the dynamical mass to its velocity dispersion

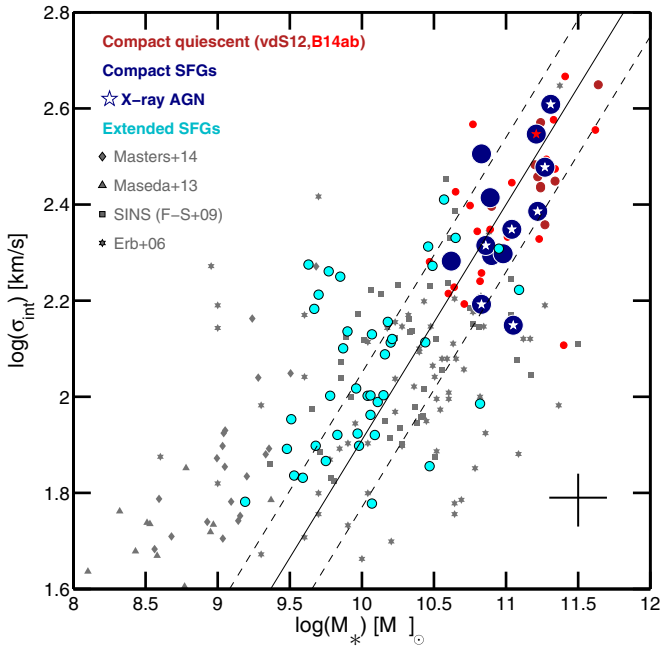

Figure 4. Distribution of $\sigma_{\rm int}$ vs. $M_\star$ for compact (blue) and extended (cyan, and gray for other references) SFGs with MOSFIRE spectra. AGN hosts are indicated with white stars. The red star depicts the galaxy in common with Belli et al. (2014b). The error bars in the bottom right corner indicate the average uncertainty in $\sigma_{\rm int}$ and $M_\star$ for compact and extended SFGs. Compact SFGs and quiescent galaxies occupy the same region of the diagram presenting a similar $M_\star$–$\sigma_{\rm int}$ correlation (solid line) with a tight scatter ($\Delta\log(\sigma_{\rm int}) = 0.14$ dex; dashed lines) over ∼1 dex in stellar mass.

(A color version of this figure is available in the online journal.)

and effective radius, through a virial factor, $K_{\rm e}$, using

$$M_{\rm dyn}(<r_{\rm e}) = K_{\rm e}\frac{\sigma_{\rm int}^2 r_{\rm e}}{G}, \quad (2)$$

the value of $K_{\rm e}$ depending on the mass density profile, the velocity anisotropy, or the shape of the gravitational potential (Courteau et al. 2014). Cappellari et al. (2006) calibrated this value from surface brightness distributions and integral field kinematics of local ellipticals, finding a Sérsic dependent factor that ranges from $K_{\rm e} = 3.6$–2.5 for low ($n = 2$) and high ($n = 5.5$) Sérsic galaxies, respectively. Similarly, Binney & Tremaine (2008) show that a factor of $K_{\rm e} = 3.35$ is appropriate for a variety of geometries and mass distributions. Here we adopt $K_{\rm e} = 2.5$, widely used in the analysis of compact quiescent galaxies at $z \sim 2$ (e.g., Newman et al. 2012; van de Sande et al. 2013; Belli et al. 2014a). We also multiply by two the value obtained with Equation (2) to indicate the *total* $M_{\rm dyn}$ instead of the mass within $r_{\rm e}$. This is a common practice in the literature, therefore in the following sections we refer to the virial constant as $K = 2K_{\rm e}$, i.e., for our calculations we use $K = 5$.

If we were to assume that compact SFGs are rotation-dominated, Equation (2) remains the same, but $\sigma_{\rm int}$ is used to infer $v_{\rm rot}$, making further assumptions on the geometry and inclination of the galaxy. In general, the virial factor in that case can vary from $K \sim 2$–10 depending on the available structural information. For spatially unresolved galaxies, the typical values range from $K \sim 3$–6 (e.g., Shapley et al. 2004; Erb et al. 2006; Maseda et al. 2013; Masters et al. 2014; also including the ×2 for the *total* $M_{\rm dyn}$) bracketing our value within a factor of a few. We use the same value for our extended SFGs to have a reference sample for which $M_{\rm dyn}$ is measured in the same way. To account for the potential uncertainty in the assumed kinematic properties of compact SFGs, we adopt a conservative error in the virial factor of 33%.

Figure 5 compares the stellar and dynamical mass estimates for our sample of compact and extended SFGs and other references from the literature spanning a broad range of stellar masses from $\log(M/M_\odot) = 8$–11. Despite the $\Delta\log(M_\star/M_{\rm dyn}) \sim 0.3$ dex scatter, the evolution in $\log(M_\star/M_{\rm dyn})$ appears to be consistent with an increasing trend as a function of stellar mass. This is clear in Figure 6 which shows the relative offset from the 1:1 relation (i.e., the stellar mass fraction) ranging from $\log(M_\star/M_{\rm dyn}) = -0.57$ dex (∼25%) at lower masses to $\log(M_\star/M_{\rm dyn}) = -0.36$ dex (∼45%) in the most massive galaxies of Förster Schreiber et al. (2009), and $\log(M_\star/M_{\rm dyn}) = -0.06^{+0.21}_{-0.13}$ dex (87^{+13}_{-18}%) in compact SFGs. This suggests that $M_\star$ is the main contributor to the dynamical mass in compact SFGs, and thus they have only small gas or dark matter fractions. Moreover, the right panel of Figure 5 shows that not only do compact SFGs and quiescent galaxies have similar integrated kinematics, but also similar, stellar-dominated, $M_{\rm dyn}$, which provides indirect evidence for the good agreement of their $r_{\rm e}(M_{\rm dyn} \sim \sigma_{\rm int}^2 r_{\rm e})$. We note that a few compact SFGs present unphysical values of $\log(M_\star/M_{\rm dyn})$, i.e., stellar masses in excess of their dynamical masses. This situation can be partially attributed to the large uncertainties in $M_{\rm dyn}$. However, there may also be second-order effects. As indicated by the arrow in Figure 5, some galaxies may require larger virial coefficient due to non-homology effects (e.g., Peralta de Arriba et al. 2014), or their σ or $r_{\rm e}$ may be slightly underestimated. For example, the most obvious outliers, 9218 and 20659, are among the most compact (higher mass density) galaxies of the sample.

It is worth mentioning that while the trend in Figure 5 depends on the virial factor, our choice of $K = 5$ is typically larger than the usual value adopted for extended SFGs (except for the few low-mass dispersion-dominated galaxies in Förster Schreiber et al. 2009; $K = 6.7$). Therefore, lowering K for compact SFGs, or increasing it for extended SFGs, would only increase the relative difference, suggesting that the mass dependence on $\log(M_\star/M_{\rm dyn})$ is not an artifact of the virial factor.

4.5. Gas and Dark Matter Fractions in Compact SFGs

Assuming that $\sigma_{\rm int}$ is dynamical in origin, the offset between $M_{\rm dyn}$ and $M_\star$ can be interpreted as evidence for other components contributing to the gravitational potential of the galaxy, such as dark matter or gas (molecular and atomic): $M_{\rm dyn} = M_\star + M_{\rm gas} + M_{\rm DM}$. In the absence of more direct measurements of the molecular gas content from CO or far-IR estimates (e.g., Daddi et al. 2010a; Magdis et al. 2012) it is unclear what the breakout is between the two contributions. In Section 4.5.1 we estimate the gas fraction if we assume that the offset in $M_{\rm dyn}$ is mainly driven by the gas content. This is a plausible assumption given that galaxies at $z \sim 2$ are known to have large gas reservoirs (Tacconi et al. 2010, 2013), and they could still be accreting gas from their parent halos (Kereš et al. 2005; Dekel & Birnboim 2006; Dekel et al. 2009). Furthermore, if massive compact galaxies become the core of local ellipticals (Bezanson et al. 2009), their dark matter fractions should be relatively small (∼10%; e.g., Cappellari et al. 2013). Nevertheless, given the assumptions above, the estimated gas fractions should be regarded as upper limits. In Section 4.5.2 we also comment

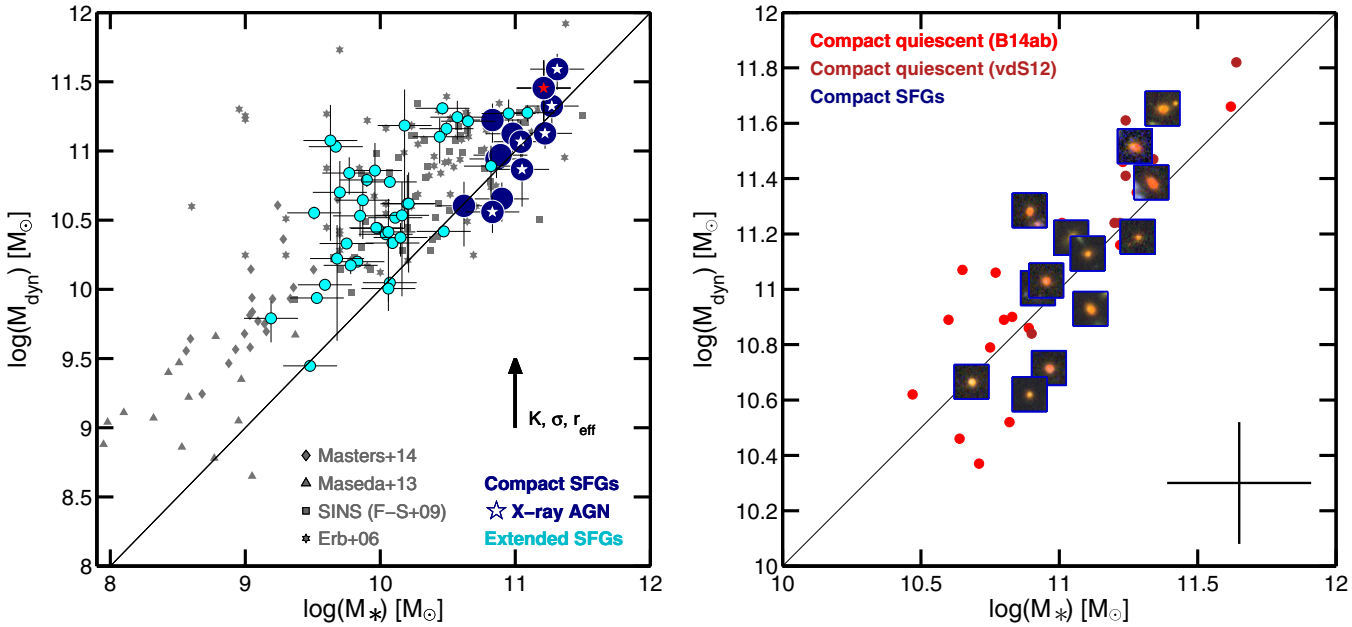

Figure 5. Left: stellar mass vs. dynamical mass of the same galaxies shown in Figure 4. The markers and colors indicate the same. The uncertainties add in quadrature a contribution from the statistical errors in size, stellar mass, and $\sigma_{\rm int}$ and the systematic uncertainty on the virial factor. We compare our measurements with the samples of intermediate- and low-mass SFGs in Maseda et al. (2013) and Masters et al. (2014), and with the more massive galaxies in Erb et al. (2006) and the SINS survey (Förster Schreiber et al. 2009). The arrow indicates the direction in which galaxies would move in the diagram as a function of increasing virial constant K, $\sigma_{\rm int}$ or $r_{\rm e}$. Right: same as left panel but focusing on the high-mass end and showing only the *zJH* color postage stamps of compact SFGs and the distribution of compact quiescent galaxies drawn from van de Sande et al. (2013) and Belli et al. (2014a, 2014b). Compact SFGs lie in the locus of compact quiescent galaxies suggesting that not only do they have similar $M_{\rm dyn} \sim M_\star$, but also consistent integrated kinematics (Figure 4) and sizes ($M_{\rm dyn} \sim \sigma_{\rm int}^2 r_{\rm e}$).

(A color version of this figure is available in the online journal.)

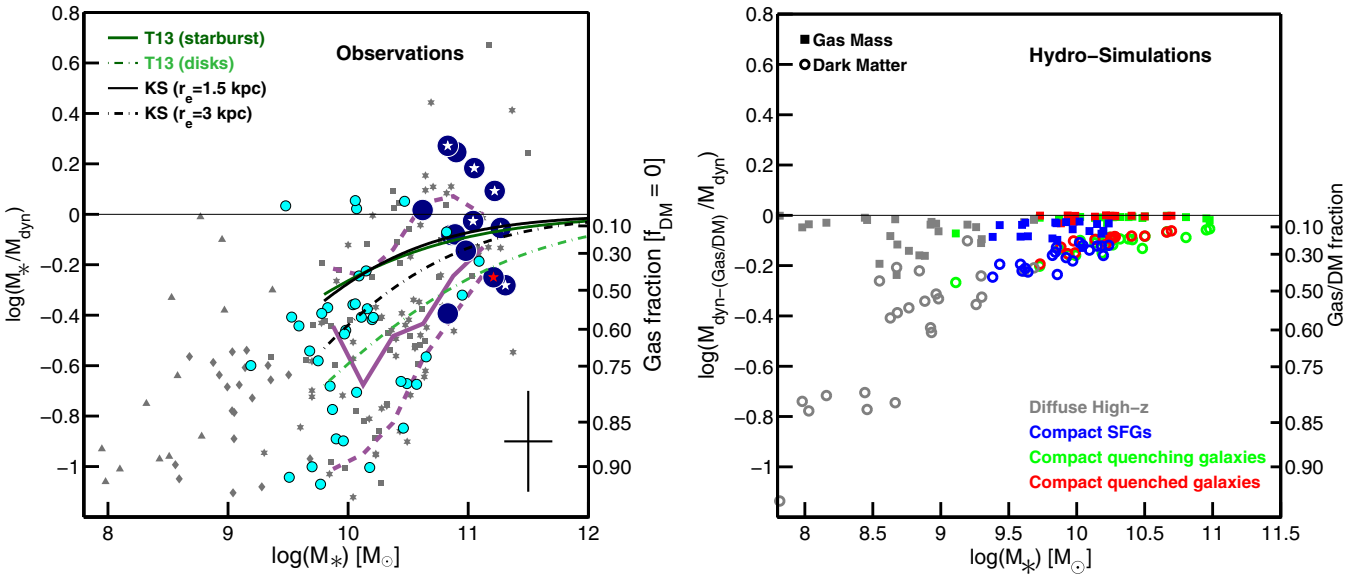

Figure 6. Left: relative offset from the $M_{\rm dyn}$ –$M_\star$ relation (i.e., stellar mass fraction) as a function of stellar mass for compact and extended SFGs. The markers and the color scheme are the same as in Figure 5. The right y-axis shows the inferred gas fraction assuming a negligible dark matter fraction, $M_{\rm dyn} = M_\star + M_{\rm gas}$. The error bars in the bottom right corner indicate the average uncertainty in $M_{\rm dyn}$ and $M_\star$ for compact and extended SFGs. The colored lines show the estimated gas fraction as a function of stellar mass from: (black) the KS relation (Kennicutt 1998) assuming either a small, $r_{\rm e} = 1.5$ (solid), or a large size, $r_{\rm e} = 3$ (dashed–dotted); (green) the log-linear KS relation of Tacconi et al. (2013) for low, $\alpha_{\rm CO} = 4.36$ (light dashed–dotted), and high, $\alpha_{\rm CO} = 1$ (dark solid), star-formation efficiencies typical of disk and starburst galaxies, respectively. The KS relation suggests that compact SFGs have lower gas fractions that extended SFGs. In practice, however, the difference is small compared to the typical uncertainties in the stellar and dynamical masses. Overall, compact SFGs have small gas fractions of ∼13% similar to those of extended SFGs of the same mass (magenta line). Right: estimated gas (square) and dark matter (circle) fractions in a sample of 30 hydrodynamical simulations from Ceverino et al. (2010) and Dekel et al. (2013). The color code indicates different evolutionary stages in the simulations starting from diffuse low-mass galaxies at $z = 4$–5 (gray) to compact SFGs (blue), compact quenching galaxies (green), and finally quiescent galaxies (red). The overall trend illustrates a similar decline in the gas and dark matter fractions with stellar mass (i.e., evolutionary stage) as in the observed galaxies. Interestingly, the models predict that the dark matter content dominates over the gas by a factor of ∼3–5 even in the most gas-rich phases.

(A color version of this figure is available in the online journal.)

on the contribution of dark matter to $M_{\rm dyn}$ from the predictions of theoretical simulations.

4.5.1. Inferred Gas Fractions

If the offset in $M_{\rm dyn}$ versus $M_\star$ reflects primarily gas content, Figure 6 suggests that the gas fraction in SFGs declines with stellar mass from $M_{\rm gas}/M_{\rm dyn} \sim 0.73$ in low-mass galaxies to $M_{\rm gas}/M_{\rm dyn} = 0.13^{+0.17}_{-0.13}$ in compact SFGs. This trend is roughly consistent with that of Tacconi et al. (2013), based on CO observations, who find a decrease in the gas fraction from $M_{\rm gas}/M_{\rm dyn} = 0.60$ to 0.35 in the stellar mass range $\log(M/M_\odot =)$ 10.4–11.2. However, at the high-mass end, our inferred gas fractions and those of other surveys such us SINS (Förster Schreiber et al. 2009) are a factor of ∼2 smaller than the CO estimates (dashed–dotted green line in Figure 6). This difference can be partially due to the large scatter and the systematic uncertainties in the virial factor or the $\alpha_{\rm CO}$ conversion (e.g., Genzel et al. 2010). However, there may be second-order effects related to the intrinsic properties of the SFGs, such as their structure or star-formation efficiencies (SFEs) of the galaxies.

Indeed, the estimated gas fractions from the Kennicutt–Schmidt (KS) relation between the gas and SFR densities (Kennicutt 1998):

$$\log(M_{\rm gas}) = 8.715 + 0.71\ \log({\rm SFR}) + 0.57 \log(r_{\rm e}) \quad (3)$$

implies that compact SFGs on the main sequence, i.e., those having similar SFRs and stellar masses as other (extended) SFGs (Figure 1, also Barro+14), would have lower $M_{\rm gas}$ simply because their sizes are up to five times smaller.

Using the best-fit to the massive ($\log(M/M_\odot) > 10$) main sequence shown in Figure 1 ($0.41(\log(M/M_\odot) - 10.5) + 1.8$; see also Whitaker et al. 2013 for a similar result) we estimate the gas fraction as a function of stellar mass and size from Equation (3). The black lines in Figure 6 indicate that the KS relation predicts smaller gas fractions by 5%–15% in extended ($r_{\rm e} \sim 3$ kpc) galaxies than in compact SFGs ($r_{\rm e} \sim 1.5$ kpc). The difference however decreases with the stellar mass, and it is small compared to the typical uncertainties indicated by the error bars in the left panel of Figure 6. Thus, around $\log(M/M_\odot) \sim 11$, the average gas fraction in compact SFGs (∼13%) and extended SFGs (magenta line) are consistent within the errors. Note also that, since the spread in the mass–size relation is smaller at the high-mass end, the difference in (size) *compactness* in the two population is not expected to be as pronounced as at lower stellar masses.

Alternatively, we can estimate the gas fraction following the empirical KS relation from Tacconi et al. (2013). In this case, the authors assume a log–linear relation, which factors out the size dependence, to provide an estimate of the SFE or gas depletion timescale, $\Sigma_{\rm SFR}/\Sigma_{\rm gas} = {\rm SFR}/M_{\rm gas} = 1/t_{\rm dep} \equiv$ SFE. Note however that the empirical relation depends on the assumed value of $\alpha_{\rm CO}$, which relates the observed $L_{\rm CO}$ to $M_{\rm gas}$. In Tacconi et al. (2013) the authors use the Milky Way conversion factor ($\alpha_{\rm CO} = 4.36$), which is appropriate for a broad range of *normal* SFGs between $z \sim 1$–2 (Daddi et al. 2008, 2010a; Genzel et al. 2012). However, this factor may be smaller in galaxies with higher SFEs similar to local (U)LIRGs or sub-mm galaxies ($\alpha_{\rm CO} \lesssim 1$; Solomon & Vanden Bout 2005; Tacconi et al. 2008; Engel et al. 2010). Several papers have indeed pointed out the presence of a population of more efficient "starburst" galaxies which are typically identified by elevated SFRs above the average main sequence (Daddi et al. 2010b; Rodighiero et al. 2011; Genzel et al. 2010; Magnelli et al. 2012). In such galaxies, the gas depletion timescales may change drastically, decreasing from $t_{\rm dep} = 0.7$ Gyr in star-forming disks (Tacconi et al. 2013; Magdis et al. 2012) to $t_{\rm dep} = 0.2$–0.3 Gyr. The green lines in Figure 6 show the evolution of the gas fraction as a function of $M_\star$ following the Tacconi et al. (2013) KS relation for low (disk-like) and high ("starburst") SFEs. The low-SFE relation is consistent with the observed distribution at lower stellar masses, but the predicted value is a factor of two larger at $\log(M/M_\odot) \sim 11$, suggesting that either a standard KS law (black lines) or a "starburst" relation provide a better match.

Interestingly, the frequency of high SFE "starburst" among massive SFGs seems to depend on the galaxy structure, such that the fraction increases among compact (or high $\sigma_{\rm int}$) galaxies (Daddi et al. 2010a; Elbaz et al. 2011; Narayanan et al. 2012). With the data at hand, we find no significant differences in the gas fraction as a function of size at a given stellar mass. However, as mentioned above, this potential difference can be better studied at low-to-intermediate stellar masses where the larger spread in the sizes of SFGs would lead to more significant variations in the gas fraction.

4.5.2. Comparison to Hydrodynamical Simulations

In the absence of 2D kinematic data and gas measurements to gauge the expected contribution of dark matter and molecular gas to $M_{\rm dyn}$, theoretical models can provide some insight on the relative contribution of each of these components. The right panel of Figure 6 shows the dark matter (circles) and gas (squares) fractions as a function of the stellar mass for a small sample of simulated galaxies at different stages of their evolution. These galaxies are drawn from the larger sample of Ceverino et al. (2010, 2014) and Dekel et al. (2013; also A. Zolotov et al. 2014, in preparation), computed with the Adaptive Refinement Tree code (Kravtsov et al. 1997) using a spatial resolution of ∼25 pc (see Ceverino & Klypin 2009 for more details about the code).

As shown in Barro et al. (2014) and Dekel & Burkert (2014), these simulated galaxies appear to describe well the formation of compact SFGs from more extended star-forming precursors that experience wet contractions as a result of mergers, violent disk instabilities, or a combination of both. The color code in the right panel of Figure 6 illustrates the evolutionary sequence from extended low-mass galaxy at high redshift (gray) to compact SFG, formed in a dissipational contraction (blue), and finally a quenching (green) or fully quiescent (red) galaxy. Each marker shows the position of a simulated galaxy in one those phases. Note, however, that due to the lack of strong quenching mechanisms, not all the simulations reach the final quiescent stage. In addition, simulated galaxies are, by selection, somewhat less massive than the observed galaxies at the compact phase (Dekel et al. 2013).

The overall trend in the simulations is qualitatively similar to the observations, illustrating the formation of a dense stellar core that becomes self-gravitating (i.e., $M_\star > M_{\rm DM}$) at the expense of turning gas into stars in the innermost region of galaxies. Interestingly, models predict the dominance of dark matter over gas even at the low-mass end where galaxies are more gas rich (15% versus 50%). In extended galaxies turning in compact, a dissipational wet inflow causes gas (and stars) to migrate inward, reaching a steady state in which gas does not accumulate in the center but slowly decreases, being turned into stars ("bathtub"), thus diluting the dark matter fraction until it reaches a base value of ∼10% (see also A. Zolotov et al. 2014, in

preparation). Although the exact gas and dark matter fractions vary from galaxy to galaxy the overall trend suggests that the dark matter content in compact SFGs is not negligible, implying that the gas fractions inferred in the previous section could be even smaller.

4.5.3. Quenching Timescales for Compact SFGs

The close agreement between $M_{\rm dyn}$ and $M_\star$ in compact SFGs implies that their gas and dark matter content must be small. The large uncertainties in $M_{\rm dyn}$ prevent a better constraint on the gas fraction, but as discussed above, unless all compact SFGs have rare intrinsic kinematics (e.g., if they are all edge-on disks), $M_{\rm dyn}$ is not underestimated by more than a factor of $\times$1.3–1.5 (i.e., K = 7–8). Furthermore, most of the other complications such as an underestimated value of $r_{\rm e}$ or an overestimated $\sigma_{\rm int}$ would move the galaxies towards smaller $M_{\rm dyn}$ and therefore gas fractions.

Taking the 13% gas fraction calculated in Section 4.5.1 at face value, and assuming no further gas accretion onto the galaxy, compact SFGs would consume their current reservoirs on timescales of $t_{\rm dep} = M_{\rm gas}/{\rm SFR} = 230^{+110}_{-190}$ Myr, where the error bars reflect the uncertainty in $M_{\rm gas}$ and SFR, as well as the small number statistics. This value fits well in the range of predicted quenching timescales required for compact SFGs to reproduce the increase in the number density of compact quiescent galaxies from $z = 3$ to $z = 2$ (Barro et al. 2013). Note also that a larger value of K does not necessarily imply longer quenching times if, as predicted by the simulations, the dark matter fraction is larger than the gas fraction in the inner regions of compact SFGs.

Most of the uncertainties in $M_{\rm dyn}$ arise from the poor constraints on the kinematic properties of the galaxies. This problem shows the obvious need for a detailed analysis of their *resolved* kinematics to quantify whether they are rotating disks or dispersion dominated galaxies. Surveys of integral field spectroscopy aided by adaptive optics (AO; Law et al. 2009; Newman et al. 2013; N. M. Förster Schreiber et al. 2014, in preparation) or high spatial resolution sub-mm observations with ALMA (e.g., Gilli et al. 2014; De Breuck et al. 2014) will shed some light on the resolved dynamics of compact SFGs, providing more precise estimates of their $M_{\rm dyn}$ and gas fractions.

4.6. Outflows from Extended Gas Regions?

The unusual formation processes responsible for compact SFGs might leave an imprint in their extended gas halos. For example, violent assembly by mergers typically leads to large (>10 kpc) gas halos (Hernquist & Mihos 1995; van Dokkum & Brammer 2010). Similarly, feedback from X-ray AGNs frequently present in compact SFGs (Barro et al. 2013; Rangel et al. 2014) would produce large extended halos of partially ionized gas, as observed around nearby quasars (Fu & Stockton 2009). While we have not found *kinematic* evidence for inflowing or outflowing gas, the gas halos might be kinematically relaxed but still visible as spatially extended emission lines.

We search for evidence of extended emission-line regions in the compact SFGs by comparing the spatial extent of the [O III]λ5007 emission line with the continuum. For sufficient signal-to-noise, we stack the spectra of compact SFGs with well-detected [O III] lines (IDs 20659, 23896, 25998, 23382, 25952, 26211, 9218). The stacked 2D spectrum is constructed by weighting each pixel in each object by the inverse of its error. The [O III] region is defined by $5004 < \lambda_{\rm rest} < 5010$, and the continuum by $4750 < \lambda_{\rm rest} < 4851$, $4871 < \lambda_{\rm rest} < 4949$, $4969 < \lambda_{\rm rest} < 4997$, and $5017 < \lambda_{\rm rest} < 5120$. The spatial profiles of the [O III] emission line and continuum are shown in Figure 7.

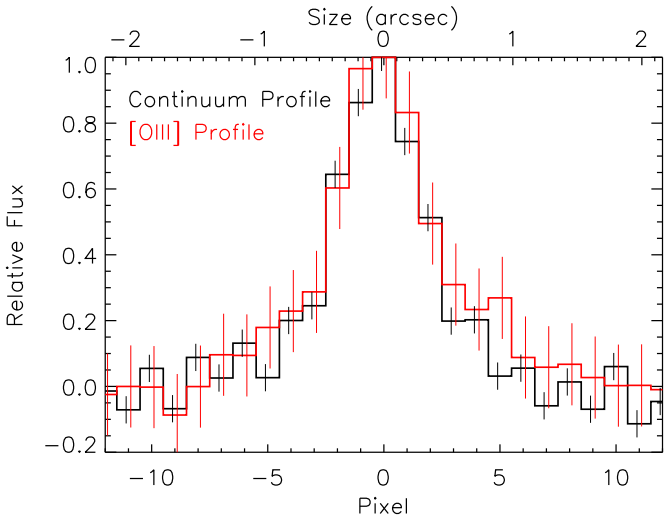

Figure 7. Spatial profiles of stacked spectra for both the continuum and [O III]λ5007 emission line. In both cases, the galaxies are marginally resolved, with FWHM ∼ 5 pixels ∼ 0.″9: larger than the typical seeing of 0.″5–0.″7. The [O III] emission line has very slightly more flux in the wings of the spatial profile, although the widths of each profile are not significantly different. In other words, our data do not show any obvious signs of a massive gas reservoir at large radii deposited by feedback or inflows.

(A color version of this figure is available in the online journal.)

The FWHMs of the two profiles are statistically consistent with one another: 5.5 ± 0.5 pixels for [O III] and 5.2 ± 0.2 pixels for the continuum. Both translate to about 0.″9 (using the MOSFIRE pixel scale of 0.″18 pixel^{-1}), slightly larger than the typical seeing (0.″5–0.″7) of the observations, which indicates that (at least some of) the galaxies are resolved in the MOSFIRE spectra. The first moment of the [O III] line (2.24 ± 0.21 pixels) is marginally larger than the continuum (1.94 ± 0.06 pixels), influenced by the excess [O III] flux in the wings of the profile (at 0.″5–1″, or ∼5–10 kpc at $z \sim 2$). However, the line width difference is not statistically significant, and thus we conclude that our compact SFGs show no obvious evidence of spatially extended excited gas.

5. SUMMARY

Using the Keck-I MOSFIRE infrared spectrograph we measure integrated velocity dispersions from the emission lines of 13 massive ($\log(M/M_\odot) \sim 10.8$), dusty (IR-bright), compact SFGs ($\Sigma_{1.5} > 10.4$) at redshift $2 \leqslant z \leqslant 2.5$ to investigate an evolutionary connection between them and compact quiescent galaxies at $z \sim 2$.

Compact SFGs have large velocity dispersions of $\sigma_{\rm int} = 230^{+40}_{-30}$ km s^{-1} consistent with the absorption-line-based measurements for a sample of equally massive quiescent galaxies at $z \sim 2$, and both populations follow a similar, tight ($\Delta\log(\sigma_{\rm int}) = 0.14$ dex), $M_\star$–$\sigma_{\rm int}$ relation over ∼1 dex in stellar mass. For one compact SFG in common with Belli et al. (2014b), the gas and stellar velocity dispersions are consistent at a 1σ level, suggesting that the width of the emission lines traces the gravitational potential. The dynamical masses of compact SFGs and quiescent galaxies are also in excellent agreement and present a small offset with respect to the $M_{\rm dyn} = M_\star$

relation, $\log(M_\star/M_{\rm dyn}) = -0.06 \pm 0.2$ dex, which is in contrast with the larger deviation found in other (extended) SFGs at the same redshift. These results suggest that: (1) compact SFGs are kinematically relaxed, i.e., the dispersion is gravitational in origin; and (2) the stellar component dominates the gravitational potential, and thus compact SFGs have only small gas or dark matter fractions. In the absence of dark matter and further gas accretion, the average gas fraction in compact SFGs (13^{+17}_{-13}%) imply short depletion timescales, $t_{\rm dep} = 230^{+110}_{-190}$ Myr.

The excellent agreement in the stellar and dynamical masses, and structural and kinematic properties of compact SFGs and quiescent galaxies, together with the a priori short quenching timescales, provide further support to the evolutionary sequence proposed in Barro et al. (2013, 2014; also Dekel & Burkert 2014), in which compact SFGs are the immediate progenitors of compact quiescent galaxies at $z \sim 2$.

This is the first observational effort aimed at studying the kinematics of massive *compact* SFGs, which represent a key phase in the formation of quiescent galaxies, but are typically absent from current spectroscopic surveys at $z \sim 2$. Our results open the door to a better characterization of these galaxies, which would require direct measurements of their intrinsic kinematics, currently unresolved in seeing-limited observations. This can be achieved either with AO-assisted NIR spectroscopy or high-resolution sub-mm observations with ALMA.

We thank Sirio Belli for useful discussions and Dan Masters for providing us with additional data for his galaxies. Support for program number HST-GO-12060 was provided by NASA through a grant from the Space Telescope Science Institute, which is operated by the Association of Universities for Research in Astronomy, Incorporated, under NASA contract NAS5-26555. G.B. acknowledges support from NSF grant AST-08-08133. P.G.P.-G. acknowledges support from grant AYA2012-31277-E. This work has made use of the Rainbow Cosmological Surveys Database, which is operated by the Universidad Complutense de Madrid (UCM), partnered with the University of California Observatories at Santa Cruz (UCO/Lick, UCSC). C.P. is supported by the KASI–Yonsei Joint Research Program (2014) for the Frontiers of Astronomy and Space Science funded by the Korea Astronomy and Space Science Institute. The authors recognize and acknowledge the very significant cultural role and reverence that the summit of Mauna Kea has always had within the indigenous Hawaiian community. We are most fortunate to have the opportunity to conduct observations from this mountain.

REFERENCES

Alexander, D. M., Bauer, F. E., Brandt, W. N., et al. 2003, AJ, 126, 539
Baldwin, J. A., Phillips, M. M., & Terlevich, R. 1981, PASP, 93, 5
Barro, G., Faber, S. M., Pérez-González, P. G., et al. 2013, ApJ, 765, 104
Barro, G., Faber, S. M., Perez-Gonzalez, P. G., et al. 2014, ApJ, 791, 52
Bell, E. F., Papovich, C., Wolf, C., et al. 2005, ApJ, 625, 23
Bell, E. F., van der Wel, A., Papovich, C., et al. 2012, ApJ, 753, 167
Belli, S., Newman, A. B., & Ellis, R. S. 2014a, ApJ, 783, 117
Belli, S., Newman, A. B., Ellis, R. S., & Konidaris, N. P. 2014b, ApJL, 788, L29
Bennert, N., Falcke, H., Schulz, H., Wilson, A. S., & Wills, B. J. 2002, ApJL, 574, L105
Bezanson, R., van Dokkum, P., van de Sande, J., Franx, M., & Kriek, M. 2013, ApJL, 764, L8
Bezanson, R., van Dokkum, P. G., Tal, T., et al. 2009, ApJ, 697, 1290
Binney, J., & Tremaine, S. 2008, Galactic Dynamics (2nd ed.; Princeton, NJ: Princeton Univ. Press)
Bothwell, M. S., Smail, I., Chapman, S. C., et al. 2013, MNRAS, 429, 3047
Brammer, G. B., van Dokkum, P. G., & Coppi, P. 2008, ApJ, 686, 1503
Brammer, G. B., Whitaker, K. E., van Dokkum, P. G., et al. 2011, ApJ, 739, 24
Bruzual, G., & Charlot, S. 2003, MNRAS, 344, 1000
Buitrago, F., Conselice, C. J., Epinat, B., et al. 2014, MNRAS, 439, 1494
Buitrago, F., Trujillo, I., Conselice, C. J., & Häußler, B. 2013, MNRAS, 428, 1460
Buitrago, F., Trujillo, I., Conselice, C. J., et al. 2008, ApJL, 687, L61
Calzetti, D., Armus, L., Bohlin, R. C., et al. 2000, ApJ, 533, 682
Cappellari, M., Bacon, R., Bureau, M., et al. 2006, MNRAS, 366, 1126
Cappellari, M., di Serego Alighieri, S., Cimatti, A., et al. 2009, ApJL, 704, L34
Cappellari, M., McDermid, R. M., Alatalo, K., et al. 2013, MNRAS, 432, 1862
Cassata, P., Giavalisco, M., Guo, Y., et al. 2011, ApJ, 743, 96
Cassata, P., Giavalisco, M., Williams, C. C., et al. 2013, ApJ, 775, 106
Ceverino, D., Dekel, A., & Bournaud, F. 2010, MNRAS, 404, 2151
Ceverino, D., & Klypin, A. 2009, ApJ, 695, 292
Ceverino, D., Klypin, A., Klimek, E., et al. 2014, MNRAS, 442, 1545
Chabrier, G. 2003, PASP, 115, 763
Chang, Y.-Y., van der Wel, A., Rix, H.-W., et al. 2013, ApJ, 773, 149
Cheung, E., Faber, S. M., Koo, D. C., et al. 2012, ApJ, 760, 131
Cimatti, A., Cassata, P., Pozzetti, L., et al. 2008, A&A, 482, 21
Courteau, S., Cappellari, M., de Jong, R. S., et al. 2014, RvMP, 86, 47
Daddi, E., Bournaud, F., Walter, F., et al. 2010a, ApJ, 713, 686
Daddi, E., Dannerbauer, H., Elbaz, D., et al. 2008, ApJL, 673, L21
Daddi, E., Elbaz, D., Walter, F., et al. 2010b, ApJL, 714, L118
De Breuck, C., Williams, R. J., Swinbank, M., et al. 2014, A&A, 565, A59
Dekel, A., & Birnboim, Y. 2006, MNRAS, 368, 2
Dekel, A., Birnboim, Y., Engel, G., et al. 2009, Natur, 457, 451
Dekel, A., & Burkert, A. 2014, MNRAS, 438, 1870
Dekel, A., Zolotov, A., Tweed, D., et al. 2013, MNRAS, 435, 999
Donley, J. L., Koekemoer, A. M., Brusa, M., et al. 2012, ApJ, 748, 142
Donley, J. L., Rieke, G. H., Pérez-González, P. G., Rigby, J. R., & Alonso-Herrero, A. 2007, ApJ, 660, 167
Elbaz, D., Dickinson, M., Hwang, H. S., et al. 2011, A&A, 533, A119
Elmegreen, B. G., & Elmegreen, D. M. 2005, ApJ, 627, 632
Elmegreen, D. M., Elmegreen, B. G., & Sheets, C. M. 2004, ApJ, 603, 74
Engel, H., Tacconi, L. J., Davies, R. I., et al. 2010, ApJ, 724, 233
Epinat, B., Tasca, L., Amram, P., et al. 2012, A&A, 539, A92
Erb, D. K., Steidel, C. C., Shapley, A. E., et al. 2006, ApJ, 647, 128
Faber, S. M., & Jackson, R. E. 1976, ApJ, 204, 668
Feldmann, R., & Mayer, L. 2014, arXiv:1404.3212
Förster Schreiber, N. M., Genzel, R., Bouché, N., et al. 2009, ApJ, 706, 1364
Förster Schreiber, N. M., Shapley, A. E., Erb, D. K., et al. 2011, ApJ, 731, 65
Franx, M., van Dokkum, P. G., Schreiber, N. M. F., et al. 2008, ApJ, 688, 770
Fu, H., & Stockton, A. 2009, ApJ, 696, 1693
Fumagalli, M., Labbe, I., Patel, S. G., et al. 2013, arXiv:1308.4132
Gallazzi, A., Charlot, S., Brinchmann, J., & White, S. D. M. 2006, MNRAS, 370, 1106
Genzel, R., Burkert, A., Bouché, N., et al. 2008, ApJ, 687, 59
Genzel, R., Förster Schreiber, N. M., Rosario, D., et al. 2014, arXiv:1406.0183
Genzel, R., Tacconi, L. J., Combes, F., et al. 2012, ApJ, 746, 69
Genzel, R., Tacconi, L. J., Gracia-Carpio, J., et al. 2010, MNRAS, 407, 2091
Gilli, R., Norman, C., Vignali, C., et al. 2014, A&A, 562, A67
Grogin, N. A., Kocevski, D. D., Faber, S. M., et al. 2011, ApJS, 197, 35
Guo, Y., Ferguson, H. C., Giavalisco, M., et al. 2013, ApJS, 207, 24
Guo, Y., Giavalisco, M., Cassata, P., et al. 2012, ApJ, 749, 149
Hernquist, L., & Mihos, J. C. 1995, ApJ, 448, 41
Holden, B. P., Oesch, P. A., Gonzalez, V. G., et al. 2014, arXiv:1401.5490
Hopkins, P. F., Hernquist, L., Cox, T. J., et al. 2006, ApJS, 163, 1
Kassin, S. A., Weiner, B. J., Faber, S. M., et al. 2007, ApJL, 660, L35
Kennicutt, R. C., Jr. 1998, ARA&A, 36, 189
Kereš, D., Katz, N., Weinberg, D. H., & Davé, R. 2005, MNRAS, 363, 2
Kirkpatrick, A., Pope, A., Charmandaris, V., et al. 2013, ApJ, 763, 123
Koekemoer, A. M., Faber, S. M., Ferguson, H. C., et al. 2011, ApJS, 197, 36
Kravtsov, A. V., Klypin, A. A., & Khokhlov, A. M. 1997, ApJS, 111, 73
Kriek, M., van Dokkum, P. G., Labbé, I., et al. 2009, ApJ, 700, 221
Krist, J. 1995, in ASP Conf. Ser. 77, Astronomical Data Analysis Software and Systems IV, ed. R. A. Shaw, H. E. Payne, & J. J. E. Hayes (San Francisco, CA: ASP), 349
Laird, E. S., Nandra, K., Pope, A., & Scott, D. 2010, MNRAS, 401, 2763
Law, D. R., Steidel, C. C., Erb, D. K., et al. 2007, ApJ, 669, 929
Law, D. R., Steidel, C. C., Erb, D. K., et al. 2009, ApJ, 697, 2057
Law, D. R., Steidel, C. C., Shapley, A. E., et al. 2012, ApJ, 745, 85
Magdis, G. E., Daddi, E., Béthermin, M., et al. 2012, ApJ, 760, 6
Magnelli, B., Lutz, D., Santini, P., et al. 2012, A&A, 539, A155
Magnelli, B., Popesso, P., Berta, S., et al. 2013, A&A, 553, A132
Maseda, M. V., van der Wel, A., da Cunha, E., et al. 2013, ApJL, 778, L22
Masters, D., & Capak, P. 2011, PASP, 123, 638

Masters, D., McCarthy, P., Siana, B., et al. 2014, ApJ, 785, 153
McLean, I. S., Steidel, C. C., Epps, H., et al. 2010, Proc. SPIE, 7735, 77351
McLean, I. S., Steidel, C. C., Epps, H. W., et al. 2012, Proc. SPIE, 8446, 84460
Michałowski, M. J., Dunlop, J. S., Cirasuolo, M., et al. 2012, A&A, 541, A85
Muzzin, A., Marchesini, D., Stefanon, M., et al. 2013, ApJ, 777, 18
Naab, T., Johansson, P. H., Ostriker, J. P., & Efstathiou, G. 2007, ApJ, 658, 710
Narayanan, D., Krumholz, M. R., Ostriker, E. C., & Hernquist, L. 2012, MNRAS, 421, 3127
Nelson, E., van Dokkum, P., Franx, M., et al. 2014, Natur, 513, 394
Newman, A. B., Ellis, R. S., Bundy, K., & Treu, T. 2012, ApJ, 746, 162
Newman, A. B., Ellis, R. S., Treu, T., & Bundy, K. 2010, ApJL, 717, L103
Newman, S. F., Genzel, R., Förster Schreiber, N. M., et al. 2013, ApJ, 767, 104
Patel, S. G., van Dokkum, P. G., Franx, M., et al. 2013, ApJ, 766, 15
Peng, C. Y., Ho, L. C., Impey, C. D., & Rix, H.-W. 2002, AJ, 124, 266
Peralta de Arriba, L., Balcells, M., Falcón-Barroso, J., & Trujillo, I. 2014, MNRAS, 440, 1634
Pérez-González, P. G., Trujillo, I., Barro, G., et al. 2008, ApJ, 687, 50
Rangel, C., Nandra, K., Barro, G., et al. 2014, MNRAS, 440, 3630
Rodighiero, G., Daddi, E., Baronchelli, I., et al. 2011, ApJL, 739, L40
Shapley, A. E., Erb, D. K., Pettini, M., Steidel, C. C., & Adelberger, K. L. 2004, ApJ, 612, 108
Solomon, P. M., & Vanden Bout, P. A. 2005, ARA&A, 43, 677
Stefanon, M., Marchesini, D., Rudnick, G. H., Brammer, G. B., & Whitaker, K. E. 2013, ApJ, 768, 92
Steidel, C. C., Rudie, G. C., Strom, A. L., et al. 2014, arXiv:1405.5473
Swinbank, A. M., Smail, I., Sobral, D., et al. 2012a, ApJ, 760, 130
Swinbank, A. M., Sobral, D., Smail, I., et al. 2012b, MNRAS, 426, 935
Szomoru, D., Franx, M., & van Dokkum, P. G. 2012, ApJ, 749, 121
Tacconi, L. J., Genzel, R., Neri, R., et al. 2010, Natur, 463, 781
Tacconi, L. J., Genzel, R., Smail, I., et al. 2008, ApJ, 680, 246
Tacconi, L. J., Neri, R., Genzel, R., et al. 2013, ApJ, 768, 74
Toft, S., Gallazzi, A., Zirm, A., et al. 2012, ApJ, 754, 3
Toft, S., Smolčić, V., Magnelli, B., et al. 2014, ApJ, 782, 68
Trujillo, I., Conselice, C. J., Bundy, K., et al. 2007, MNRAS, 382, 109
Trump, J. R., Konidaris, N. P., Barro, G., et al. 2013, ApJL, 763, L6
Trump, J. R., Weiner, B. J., Scarlata, C., et al. 2011, ApJ, 743, 144
Tully, R. B., & Fisher, J. R. 1977, A&A, 54, 661
Utomo, D., Kriek, M., Labbe, I., Conroy, C., & Fumagalli, M. 2014, ApJL, 783, L30
van de Sande, J., Kriek, M., Franx, M., et al. 2013, ApJ, 771, 85
van der Wel, A., Bell, E. F., Häussler, B., et al. 2012, ApJS, 203, 24
van der Wel, A., Franx, M., van Dokkum, P. G., et al. 2014, ApJ, 788, 28
van der Wel, A., Rix, H.-W., Wuyts, S., et al. 2011, ApJ, 730, 38
van Dokkum, P. G., & Brammer, G. 2010, ApJL, 718, L73
van Dokkum, P. G., Franx, M., Kriek, M., et al. 2008, ApJL, 677, L5
Wake, D. A., van Dokkum, P. G., & Franx, M. 2012, ApJL, 751, L44
Weiner, B. J., Willmer, C. N. A., Faber, S. M., et al. 2006, ApJ, 653, 1027
Whitaker, K. E., Labbé, I., van Dokkum, P. G., et al. 2011, ApJ, 735, 86
Whitaker, K. E., van Dokkum, P. G., Brammer, G., et al. 2013, ApJL, 770, L39
Williams, C. C., Giavalisco, M., Cassata, P., et al. 2014a, ApJ, 780, 1
Williams, R. J., Maiolino, R., Santini, P., et al. 2014b, arXiv:1405.3664
Wuyts, S., Cox, T. J., Hayward, C. C., et al. 2010, ApJ, 722, 1666
Wuyts, S., Förster Schreiber, N. M., Genzel, R., et al. 2012, ApJ, 753, 114
Wuyts, S., Förster Schreiber, N. M., Lutz, D., et al. 2011a, ApJ, 738, 106
Wuyts, S., Förster Schreiber, N. M., van der Wel, A., et al. 2011b, ApJ, 742, 96
Xue, Y. Q., Luo, B., Brandt, W. N., et al. 2011, ApJS, 195, 10